Published in final edited form as:
Nat Nanotechnol. ; 6(11): 720–725. doi:10.1038/nnano.2011.160.

Nanowired three dimensional cardiac patches

Tal Dvir[1,2,†], **Brian P. Timko**[1,2,†], **Mark D. Brigham**[3], **Shreesh R. Naik**[1], **Sandeep S Karajanagi**[1,4], **Oren Levy**[5,6], **Hongwei Jin**[3], **Kevin K. Parker**[3], **Robert Langer**[1], and **Daniel S. Kohane**[2,*]

[1]Department of Chemical Engineering, Massachusetts Institute of Technology, Cambridge, MA 02139

[2]Laboratory for Biomaterials and Drug Delivery, Department of Anesthesiology, Division of Critical Care Medicine, Children's Hospital Boston, Harvard Medical School, 300 Longwood Avenue, Boston, Massachusetts 02115

[3]Disease Biophysics Group, Wyss Institute for Biologically-Inspired Engineering, School of Engineering and Applied Sciences, Harvard University, Cambridge, Massachusetts 02138

[4]Department of Surgery, Massachusetts General Hospital, Harvard Medical School, Boston, Massachusetts 02114

[5]Harvard-Massachusetts Institute of Technology Division of Health Sciences and Technology, Cambridge, MA 02139

[6]Department of Medicine, Brigham and Women's Hospital, Harvard Medical School, Cambridge, Massachusetts 02139

Engineered cardiac patches for treating damaged heart tissues after a heart attack are normally produced by seeding heart cells within three dimensional porous biomaterial scaffolds[1–3]. These biomaterials, which are usually made of either biological or synthetic polymers, help cells organize into functioning tissues but the poor conductivity of these materials limits the patch from contracting strongly as a unit. Here we show that incorporating gold nanowires within alginate scaffolds can bridge the electrically resistant pore walls of alginate and improve electrical communication between adjacent cardiac cells. When electrically stimulated, cells grown on the modified matrices could contract synchronously, and tissues were thicker and better aligned than those grown on pristine alginate. Furthermore, higher levels of proteins involved in muscle contraction and electrical coupling were detected in the composite matrices. It is expected that integration of conducting nanowires within three dimensional scaffolds may improve the therapeutic value of current cardiac patches.

The urgent need to improve the viability, ultrastructural morphology and functionality of engineered cardiac tissue has been addressed by developing bioreactors that can provide enhanced mass transfer[4,5] or expose tissues to electrical[6] and mechanical cues[7,8]. Structural and mechanical properties of scaffolds have been improved by microfabrication processes that control stiffness and anisotropy[9]. Nanostructures incorporated into matrices foster tissue

*To whom correspondence should be addressed, Daniel.Kohane@childrens.harvard.edu.
†Equal contribution

Author contributions T.D. and B.P.T. conceived the idea. T.D., B.P.T., K.K.P., R.L. and D.S.K. designed experiments and interpreted data. T.D., B.P.T., M.D.B., S.R.N., S.S.K. and O.L. performed the experiments. H.J. analyzed data. T.D., B.P.T., and D.S.K. co-wrote the paper.

Additional information The authors declare no competing financial interests. Supplementary information accompanies this paper at www.nature.com/naturenanotechnology. Reprints and permission information is available online at http://www.nature.com/reprints/.

morphogenesis and functionality, improve mechanical and adhesive properties, and direct cells to self-assemble in 3D[10–13].

The key limitation of porous matrices used for cardiac tissue engineering addressed here is that their pore walls limit cell-cell interaction and delay electrical signal propagation[14]. We developed 3D nanocomposites of gold nanowires (NWs) within macroporous alginate scaffolds, to bridge the non-conducting pore walls, increase electrical signal propagation throughout the cell-seeded scaffold, and enhance the organization of functioning tissue (Fig. 1). Inorganic nanostructures interact with cardiomyocytes and neurons, e.g. to create electronic interfaces[15–17] and enhance cellular excitability[18,19]. Gold nanoparticles are promising candidates for tissue engineering since they can be designed to minimize toxicity[20] and have been used in drug delivery, imaging and cancer therapy[21]. Such a nanocomposite cellular construct could subsequently be sutured on the infarcted heart to restore function[2]. In time the scaffold will degrade, leaving nanowires embedded within the engineered tissue.

Alginate was selected as a model scaffold material because it has been used extensively in myocardial regeneration[1,2,22–24], and has been approved for Phase II clinical trials for treating myocardial infarction (MI)[25]. Like other common scaffolds (collagen, PLGA and PGS), alginate scaffolds exhibit defined porous structures and favorable biocompatibility, but lack electrical conductivity.

Nanowires should be longer than the average thickness of the alginate pore wall (~ 500 nm) to interact with cells on both sides, and to enhance electrical signal transmission throughout the scaffold. NWs synthesized by anisotropic gold seed elongation[26,27], had average lengths of 1 μm, diameters of 30 nm (Fig. 2a, b; Supplementary Fig. S1), and zeta potentials of +45 ± 3 mV because of the hexadecyltrimethylammonium bromide (CTAB) capping agent.

A nanocomposite scaffold of alginate and NWs (Alg-NW) was created by mixing NWs with sodium alginate, then cross-linking with calcium ions and lyophilizing (Supplementary Fig. S2). Rheology of the alginate gel prior to lyophilization showed increased dynamic viscosity and elastic shear modulus with NW concentration (Supplementary Fig. S3). Nanocomposites exhibit improved mechanical properties because the nanomaterials, which interact with the polymers[28], act as reinforcements[29,30]. Here, the positively-charged gold NWs may have interacted electrostatically with the alginate.

The compressive modulus (Ec) of the wet scaffolds was measured to evaluate their ability to accommodate compressive strain from cardiac beating. The Ec for alginate and Alg-NW nanocomposites were 1.2 ± 0.2 and 3.5 ± 0.2 kPa, respectively (p= 0.008) which is significantly lower than that of the native heart (Ec = 425 ± 9 kPa, $p < 0.001$). Because similar Ec values have been measured for decellularized cardiac matrices[31], it is unlikely that Alg-NW scaffolds will inhibit contraction in the engineered tissue. Moreover, scaffolds with lower Ecs have been shown to support cardiac cells and promote the organized beating of cardiac tissues[2,8]. As the scaffold degrades and extracellular matrix is produced, the microenvironment will eventually resemble that of native tissue.

Scanning electron microscopy of scaffolds revealed that at 0.5 mg/mL, NWs either were parallel to or penetrated the pore walls (Supplementary Fig. S4a). At 1 mg/mL, the wires formed star-shaped aggregates inside the walls 5 μm in scale (Fig. 2c, d). Elemental analysis confirmed they contained gold (Supplementary Fig. S4b). At these concentrations NWs were homogenously distributed about 5–10 μm apart throughout the scaffold.

To simulate the pore wall of the Alg-NW scaffold and to evaluate the bridging effect of the NWs on the spatial conductivity of the alginate surfaces, we coated approximately 500 nm-

thick films of Alg-NW on indium tin oxide conducting glass slides and measured the surface topography and film conductance by conductive atomic force microscopy (Fig. 3a– d). The many coincident features in the topography and conductance plots indicated that nanowires fully bridged the film. Since the length of the NWs was not monodisperse and their orientation was random within the films, topographic and conductive coincidences were not identical. At the NWs, current was proportional to voltage bias over the range of −1 to 1V, while negligible current passed through NW-free regions of the film (Fig. 3e). Higher concentrations of NWs (2 mg/mL) increased conductive coincident features (Supplementary Fig. S5a, b). Alginate films containing gold nanorods significantly shorter than the film thickness (average length ~60 nm; Supplementary Fig. S6a), showed topographic features similar to those containing NWs, but negligible electrical current was detected (Supplementary Fig. S6b–d).

Further evidence of enhanced conductivity from NWs was obtained by measuring the overall film impedance. Films were pressed between two indium tin oxide electrodes and an AC bias was swept between 1 MHz and 1 Hz (Fig. 3f). All films exhibited relatively low impedance at high frequencies (>10 kHz) due to capacitive currents through the film. At lower frequencies that encompass the frequency spectrum of mammalian heart rates (order of 1 Hz), Alg-NW impedance was consistently lower than in pristine films, a finding attributable to resistive currents through the bridging nanowires becoming increasingly dominant as capacitive currents drop off[32].

We isolated cardiac cells (cardiomyocytes and fibroblasts) from the left ventricles of neonatal rat hearts and seeded them into Alg-NW or pristine alginate scaffolds (Supplementary Methods). The effect of NWs on the organization of cardiac cells was studied after culture for 3 days under static conditions (without electrical stimulation), and again after 5 days of cultivation under electrical field stimulation to improve cell alignment[6]. Typically, cardiac cells seeded in pristine alginate scaffolds do not bind to the matrix, but organize into tight, rounded aggregates (< 200 μm) within the pores[8]. Hematoxylin and eosin (H&E) staining at day 8 revealed thick, intact and better-aligned tissues within the Alg-NW scaffolds (Fig. 4a,b) compared to the small aggregates within alginate scaffolds (Fig. 4c, d). On day 8, NWs were seen in pore walls (Fig. 4e), suggesting that NWs remained integrated throughout the cultivation period. H&E-stained thin sections of scaffolds seeded with fewer cells revealed wires in scaffold walls in close proximity to cell bundles in adjacent pores (Fig. 4f). Based on a metabolic activity assay, neither the NWs nor their residual chemicals had any cytotoxic effects on the cardiac cells (Supplementary Fig. S7). In vivo studies will be crucial for definitive demonstration of biocompatibility.

The phenotype of the engineered tissue was evaluated by immunostaining for troponin I, which is involved in muscle calcium binding and contraction, and for the gap junction protein connexin 43 (Cx-43), which is responsible for electrical and mechanical coupling[8]. On day 3 (before stimulation), cardiomyocytes within the Alg-NW scaffold expressed higher levels of both proteins (Supplementary Fig. S8a,b). Immunostaining on day 8 revealed strong troponin I fluorescence and cells located throughout the Alg-NW scaffolds (Fig. 4g), but not in the pristine scaffolds (Fig. 4h). In the Alg-NW cultures, Cx-43 between adjacent cardiomyocytes suggested maturation of the tissue (Fig 4i); this was not seen with unmodified matrices. Western blotting revealed that the Alg-NW cultures had significantly higher amounts of Cx-43 and α-sarcomeric actinin (a protein related to contractile function[8]) at days 3 and 8 (Figs. 4j,k and Supplementary Fig. S8c). This means the NWs imparted phenotypic traits consistent with enhanced electrical and mechanical coupling and contractile properties. The higher Cx-43 level in the Alg-NW scaffold on day 3, before electrical stimulation, suggests that the wires affect physiology independently of possible complementary effects of the external electrical field.

Assessment of the electrophysiological effects of NWs was performed in cardiac cell constructs, with or without NWs, incubated with a calcium-sensitive dye. Isolated cardiac cell aggregates from each group were stimulated with a local electrical field using microelectrodes. The propagation and green fluorescence intensity of the dye in the engineered tissue were recorded videographically and plotted (Fig. 5). Similar behavior was observed for 6 separate constructs in each group. Calcium imaging within pristine scaffolds revealed activity only at the stimulation site, with negligible signal propagation to cells in adjacent pores (Supplementary Movie M1, Fig. 5a, b). Analysis of the recording at six separate sites (Fig. 5a, white circles I–VI) revealed calcium transients only at the stimulus point (I) but not at the nearest other point (II), slightly more than 100 μm away (Fig. 5b). In contrast, the engineered tissue in the Alg-NW scaffolds contracted synchronously (Supplementary Movie M2, Fig 5c, d); note the stimulation point was 2 mm to the lower left of point I (i.e. far off the lower left corner of the graphic). In contrast to the lack of signal conduction in the absence of NWs, here recordings at various sites (Fig. 5c, white circles I–V) revealed calcium transients (Fig. 5d) throughout the scaffold, even though the stimulation point was remote. The calcium transients at sites I–V occurred in a temporal sequence determined by their spatial relationship to the source of stimulation (Fig. 5e), suggesting continuous propagation of a wave-front of cell depolarization. Furthermore, the calcium transients in the Alg-NW group were significantly higher than in the pristine scaffolds (Fig. 5f).

Many factors may have contributed to the improved scaffold functionality. NWs may create conductive bridges across the alginate, connecting adjacent pores and/or cell bundles. Alternatively, the nanowires may directly enhance expression of the electrical coupling protein Cx-43. The improvement in tissue thickness and contractile properties may enhance electrical connectivity and functionality. Since the NWs were not interconnected structurally (Figs. 2, 4e–f) or electrically (Figs. 3, S5), long-range shorting throughout the construct is unlikely. Finally, the effects of NWs on the viability of fibroblasts that could also be found in the seeded scaffolds, and the secretion of extracellular matrix by those fibroblasts, may also have impacted the functional enhancements observed.

We demonstrate for the first time that nanocomposites of inorganic nanomaterials in polymeric matrices can be used to enhance the structure, phenotype, and function of engineered cardiac tissue. Our approach may be useful in creating more homogenous cardiac patches with stronger contractile properties that would be implanted on the affected surface of a heart after MI. This technique could be generalized to other biomaterials such as elastomers or electrospun fibers, and to diseases of other conductive tissues.

Methods

Preparation of gold NWs

All chemicals were acquired from Sigma-Aldrich (St. Louis, MO) and used as-received. Nanowires were prepared using an adaption of previously reported methods.[26,27] First, citrate-capped Au seeds were prepared. A 20 mL aqueous solution of $HAuCl_4$ (0.25 mM) and sodium citrate (0.25 mM) was prepared. Under vigorous stirring, 0.6 mL ice-cold aqueous $NaBH_4$ solution (0.1 M) was added all at once. The solution immediately turned deep red, consistent with the formation of colloidal gold. A typical product contained spherical gold particles ca. 4 nm in diameter at an estimated density of ca. 7.6×10^{13} particles/ml. The suspension was allowed to stand at RT for several hours before use to ensure complete degradation of the $NaBH_4$. The gold colloid was stable at 4°C for at least several months.

Wires were grown by anisotropic elongation of the seeds. To achieve high aspect ratio nanowires, the reaction was carried out in three stages, in 25-ml Erlenmeyer flasks (Flasks A and B) and a 250-ml round-bottom flask (Flask C). First, Growth Solution was prepared. 7.54 g CTAB (0.1 M) was dissolved in 200 ml DI water at 37°C. After complete dissolution of the CTAB, $HAuCl_4$ was added (0.25 mM) followed by ascorbic acid (0.5 mM). The ascorbic acid changed the solution from deep to pale yellow, consistent with the reduction of Au(III) to Au(I). Finally, HNO_3 (70 mM) was added. The Growth Solution was then divided between Flask A (9 mL), Flask B (18 mL), and Flask C (173 mL). Nanowire growth was initiated by adding 1 mL Seed Solution to Flask A under vigorous stirring. After 15 s, 1 mL solution was transferred from Flask A to Flask B, with vigorous stirring. After 30 s, 5 mL solution was transferred from Flask B to Flask C, with vigorous stirring. The solution in Flask C was maintained at 37°C with stirring, and turned deep purple over the course of 2 hrs. The solution contained a mixture of morphologies and was subsequently purified. The solution was collected in 50-mL centrifuge tubes, which were then situated in a 37°C oven undisturbed for ca. 1 week. During this time, a brown pellet, which contained ca. 90% wires, formed at the bottom of each tube. The supernatant was discarded, and the pellets were resuspended in DI water. A typical synthesis yielded ca. 60 mg product after purification.

Preparation of Alg-NW and alginate scaffolds

The 3D Alg-NW or alginate scaffolds were prepared from pharmaceutical grade alginate, Protanal LF 5/60 (FMC Biopolymers, Drammen, Norway), which has a high guluronic acid (G) content (65%). The method for Alg-NW scaffold preparation is based on a previously described procedure[8] and is a five-step process, consisting of: (i) preparation of sodium alginate stock solutions at concentrations of 1% (w/v); (ii) mixing NW solution (1 mg/mL) with the alginate solution followed by rapid mixing (iii); crosslinking of the alginate/NW solution by adding the bivalent cross-linker (e.g., calcium gluconate); (iv) freezing the cross-linked alginate in a homogeneous, cold (−20°C) environment; and (v) lyophilization to produce a sponge like scaffold (5 mm × 2 mm, d × h). The scaffolds were sterilized with UV light before use and were 90% porous with pore sizes ranging from 50 to 100 μm in diameter[8]. Alginate scaffolds were prepared in the same manner without step (ii).

Intracellular calcium transient measurement

Neonatal rat ventricular myocytes were incubated with 10 μM fluo-4 AM (Invitrogen) and 0.1 % Pluronic F-127 for 45 min at 37 °C. Cardiac cell constructs (at least 6 samples from each group, from 3 separate experiments) were subsequently washed 3 times in modified Tyrode solution to allow de-esterification. Cell aggregates were electrically paced at 1–2Hz using a bipolar platinum electrode placed in close contact with the cells using a micromanipulator. The calcium transients were imaged using a confocal imaging system (LSM 510, Zeiss). The images were acquired with a EC Plan-Neofluar 10× /0.30M 27 objective lens at 216 frame/s 256×256 pixels and 2.5 μm/pixel spatial resolution. Fluo 4 was excited at 488 nm diode laser. Fluorescence (F) was normalized by dividing by the basal cell fluorescence (F0) after dye loading. Calcium transient traces were plotted in Igor Pro. For comparison of expanded sections (Figure 5e), the background noise was reduced using the binomial smoothing algorithm within Igor Pro. For quantification, the intensity maximum of fluorescence was measured using ImageJ software at a point 2 mm from the stimulation spot, for 6 separate samples in each group.

Statistical analysis

Data are presented as means ± S.D. Univariate differences between the groups were assessed with Student's t test. All analyses were performed using GraphPad Prism version 5.00 for Windows (GraphPad Software, San Diego, CA). $P < 0.05$ was considered significant.

Supplementary Material

Refer to Web version on PubMed Central for supplementary material.

Acknowledgments

This research was funded by NIH Grants GM073626 (to D.S.K) and DE13023 and DE016516 (to R.L). T.D thanks the American Heart Association for a Postdoctoral Fellowship. B.P.T. acknowledges an NIH Ruth L. Kirschstein National Research Service Award, Number F32GM096546. We would like to thank Hyoungshin Park, Bozhi Tian, David Liu, Avni Argun and Leon Bellan for their assistance and discussion.

References

1. Leor J, et al. Bioengineered cardiac grafts: A new approach to repair the infarcted myocardium? Circulation. 2000; 102:III56–61. [PubMed: 11082363]
2. Dvir T, et al. Prevascularization of cardiac patch on the omentum improves its therapeutic outcome. Proceedings of the National Academy of Sciences of the United States of America. 2009; 106:14990–14995. [PubMed: 19706385]
3. Zimmermann WH, et al. Engineered heart tissue grafts improve systolic and diastolic function in infarcted rat hearts. Nature Medicine. 2006; 12:452–458.
4. Dvir T, Benishti N, Shachar M, Cohen S. A novel perfusion bioreactor providing a homogenous milieu for tissue regeneration. Tissue Engineering. 2006; 12:2843–2852. [PubMed: 17518653]
5. Radisic M, et al. Medium perfusion enables engineering of compact and contractile cardiac tissue. Am J Physiol Heart Circ Physiol. 2004; 286:H507–516. [PubMed: 14551059]
6. Radisic M, et al. Functional assembly of engineered myocardium by electrical stimulation of cardiac myocytes cultured on scaffolds. Proceedings of the National Academy of Sciences of the United States of America. 2004; 101:18129–18134. [PubMed: 15604141]
7. Zimmermann WH, et al. Tissue engineering of a differentiated cardiac muscle construct. Circulation Research. 2002; 90:223–230. [PubMed: 11834716]
8. Dvir T, Levy O, Shachar M, Granot Y, Cohen S. Activation of the ERK1/2 cascade via pulsatile interstitial fluid flow promotes cardiac tissue assembly. Tissue Engineering. 2007; 13:2185–2193. [PubMed: 17518740]
9. Engelmayr GC, et al. Accordion-like honeycombs for tissue engineering of cardiac anisotropy. Nature Materials. 2008; 7:1003–1010.
10. Dvir T, Timko BP, Kohane DS, Langer R. Nanotechnological strategies for engineering complex tissues. Nat Nanotechnol. 2011; 6:13–22. [PubMed: 21151110]
11. Sachlos E, Gotora D, Czernuszka JT. Collagen scaffolds reinforced with biomimetic composite nano-sized carbonate-substituted hydroxyapatite crystals and shaped by rapid prototyping to contain internal microchannels. Tissue Eng. 2006; 12:2479–2487. [PubMed: 16995781]
12. Souza GR, et al. Three-dimensional tissue culture based on magnetic cell levitation. Nat Nanotechnol. 5:291–296. [PubMed: 20228788]
13. Wu SL, et al. A Biomimetic Hierarchical Scaffold: Natural Growth of Nanotitanates on Three-Dimensional Microporous Ti-Based Metals. Nano Letters. 2008; 8:3803–3808. [PubMed: 18950232]
14. Bursac N, Loo YH, Leong K, Tung L. Novel anisotropic engineered cardiac tissues: Studies of electrical propagation. Biochemical and Biophysical Research Communications. 2007; 361:847–853. [PubMed: 17689494]
15. Timko BP, et al. Electrical Recording from Hearts with Flexible Nanowire Device Arrays. Nano Letters. 2009; 9:914–918. [PubMed: 19170614]
16. Timko BP, Cohen-Karni T, Qing Q, Tian BZ, Lieber CM. Design and Implementation of Functional Nanoelectronic Interfaces With Biomolecules, Cells, and Tissue Using Nanowire Device Arrays. Ieee Transactions on Nanotechnology. 2010; 9:269–280. [PubMed: 21785576]
17. Tian B, et al. Three-dimensional, flexible nanoscale field-effect transistors as localized bioprobes. Science. 329:830–834. [PubMed: 20705858]

18. Lovat V, et al. Carbon nanotube substrates boost neuronal electrical signaling. Nano Letters. 2005; 5:1107–1110. [PubMed: 15943451]
19. Cellot G, et al. Carbon nanotubes might improve neuronal performance by favouring electrical shortcuts. Nature Nanotechnology. 2009; 4:126–133.
20. Khlebtsov N, Dykman L. Biodistribution and toxicity of engineered gold nanoparticles: a review of in vitro and in vivo studies. Chem Soc Rev. 2011; 40:1647–1671. [PubMed: 21082078]
21. Giljohann DA, et al. Gold nanoparticles for biology and medicine. Angew Chem Int Ed Engl. 2010; 49:3280–3294. [PubMed: 20401880]
22. Hao XJ, et al. Angiogenic effects of sequential release of VEGF-A(165) and PDGF-BB with alginate hydrogels after myocardial infarction. Cardiovascular Research. 2007; 75:178–185. [PubMed: 17481597]
23. Yu J, et al. The effect of injected RGD modified alginate on angiogenesis and left ventricular function in a chronic rat infarct model. Biomaterials. 2009; 30:751–756. [PubMed: 19010528]
24. Ruvinov E, Leor J, Cohen S. The promotion of myocardial repair by the sequential delivery of IGF-1 and HGF from an injectable alginate biomaterial in a model of acute myocardial infarction. Biomaterials. 2011; 32:565–578. [PubMed: 20889201]
25. ClinicalTrials.gov. ID: NCT01226563
26. Gole A, Murphy CJ. Seed-mediated synthesis of gold nanorods: Role of the size and nature of the seed. Chemistry of Materials. 2004; 16:3633–3640.
27. Kim F, Sohn K, Wu JS, Huang JX. Chemical Synthesis of Gold Nanowires in Acidic Solutions. Journal of the American Chemical Society. 2008; 130:14442–+. [PubMed: 18850710]
28. Mitamura K, Imae T, Saito N, Takai O. Fabrication and self-assembly of hydrophobic gold nanorods. J Phys Chem B. 2007; 111:8891–8898. [PubMed: 17625825]
29. Tjong SC. Structural and mechanical properties of polymer nanocomposites. Mater. Sci. Eng. R-Rep. 2006; 53:73–197.
30. Balazs AC, Emrick T, Russell TP. Nanoparticle polymer composites: where two small worlds meet. Science. 2006; 314:1107–1110. [PubMed: 17110567]
31. Godier-Furnemont AF, et al. Composite scaffold provides a cell delivery platform for cardiovascular repair. Proc Natl Acad Sci U S A. 2011
32. Horowitz, P.; Hill, W. The art of electronics. Cambridge University Press; Cambridge [England]: New York: 1989.

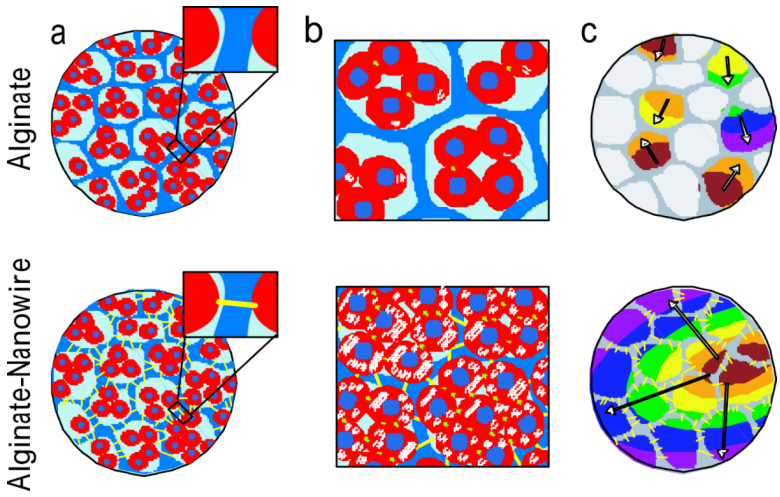

Figure 1. Schematic overview of 3D nanowired cardiac tissue

a, Isolated cardiomyocytes are cultured in either pristine alginate or Alg-NW composites. Insets highlight the components of the engineered tissue: cardiac cells (red), alginate pore wall (blue) and gold nanowires (yellow). **b,** Whereas cardiomyocytes in pristine alginate scaffolds (top) typically form only small clusters that beat asynchronously and with random polarization, Alg-NW scaffolds (bottom) could exhibit synchronization across scaffold walls, throughout the entire scaffold. Colors, contour lines, and arrow represent the spatial and temporal evolution of signal maximum. **c,** Cardiomyocytes cultured in alginate scaffolds (top) form small beating clusters, but synchronously-beating cardiomyocytes in Alg-NW composites (bottom) have the potential to form organized cardiac-like tissue.

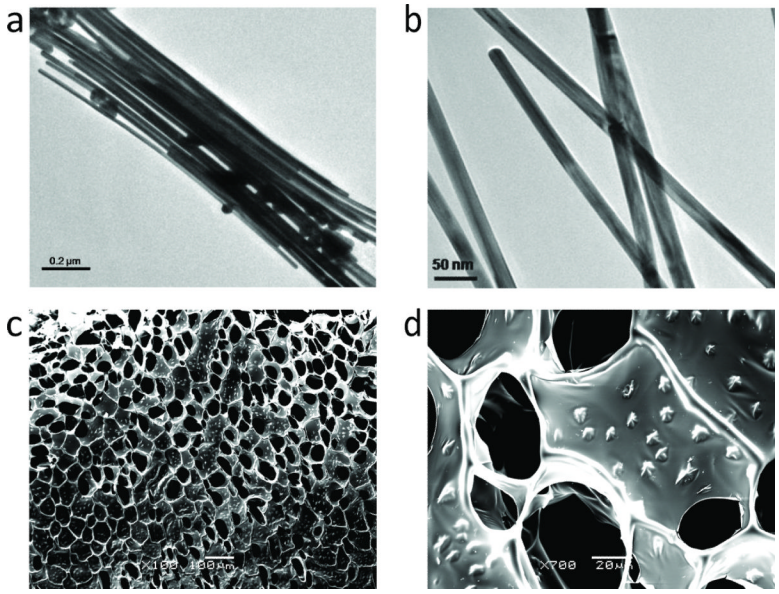

Figure 2. Incorporation of NWs within alginate scaffolds

a, and b, TEM images of a typical distribution of gold nanowires. The NWs exhibited an average length of ~1 μm and an average diameter of 30 nm. **c, and d,** SEM revealed that the NWs (1 mg/mL) assembled within the pore walls of the scaffold into star-shaped structures with a total length scale of 5 μm. The assembled wires were distributed homogenously within the matrix (c) with a distance of approximately 5 μm from each other (d).

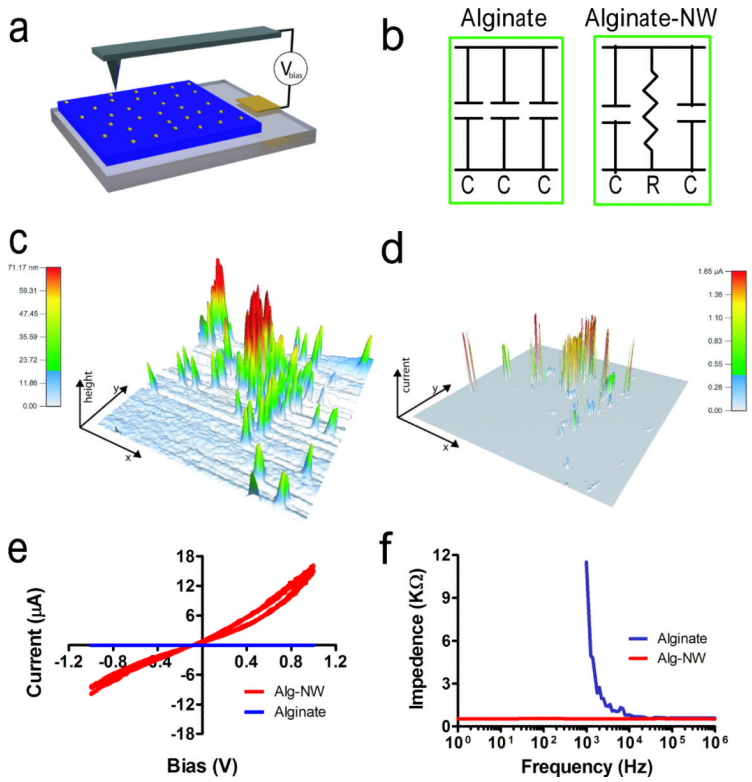

Figure 3. Increased electrical conductivity of alginate by incorporation of NWs

a, Spatial conductivity was measured by conductive probe atomic force microscopy (C-AFM). The ITO slide served a backside contact, while the conductive AFM probe was used to simultaneously measure surface topography and conductance through the film. **b,** The equivalent circuit can be represented by capacitors (alginate) and resistors (NWs) connected in parallel. **c,** Topographic mapping revealed NWs protruding from the composite alginate thin film (5×5 μm). **d,** Spatial conductivity within the Alg-NW film as measured by C-AFM. Current spikes were measured at the location of the NWs. **e,** Current measured at the NWs (red) increased with bias voltage over the range −1 to 1V, while negligible current passed through NW-free regions of the alginate film (blue) over that same range. **f,** Overall impedance of the scaffold biomaterial before and after modification with NWs. Thin layers of Alg-NW or pure alginate films were pressed between two ITO glass slides. These slides served as electrodes and were used to apply an AC bias with frequency swept between 1 MHz and 10 Hz. At frequencies near DC, the impedance of the composite membrane was much lower than that of the pure film.

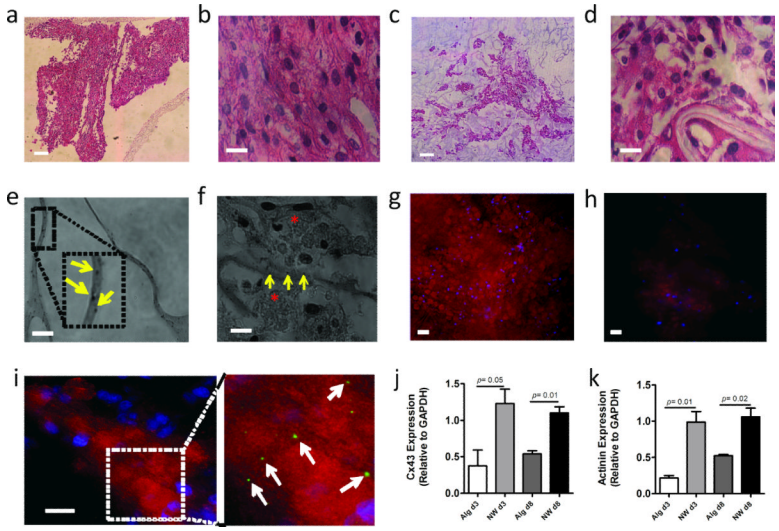

Figure 4. Cardiac cell organization within the 3D scaffold

a– d, H&E stained sections of thin sections of the engineered tissues on day 8 revealed a thick tissue in the NW scaffold (a, b) while the engineered tissue in the pristine scaffolds revealed non-continuous tissue separated by pore walls (c, d). NWs are seen within the pore walls of a relatively empty region of a scaffold (black dots indicated by yellow arrows) **e,** In a sparsely populated region, wires within the wall (black dots indicated by yellow arrows) were in close proximity to cell aggregates (red asterisks) (f). **g–h,** Immunostaining of the cell seeded scaffolds on day 8 revealed pervasive troponin I expression (red) within the Alg-NW scaffold (g), while less staining was observed in the aggregates in the un-modified scaffolds (h). **i,** Connexin 43 gap junction protein was found between cardiomyocytes in the NW-containing scaffolds (green dots indicated by white arrows). Nuclei are colored in blue. **j,** Quantification of connexin 43 protein expression by Western blot. k. Quantification of sarcomeric actinin protein expression by Western blot. Scale bars are 200 μm (a,c) or 20 μm (b,d,e–i).

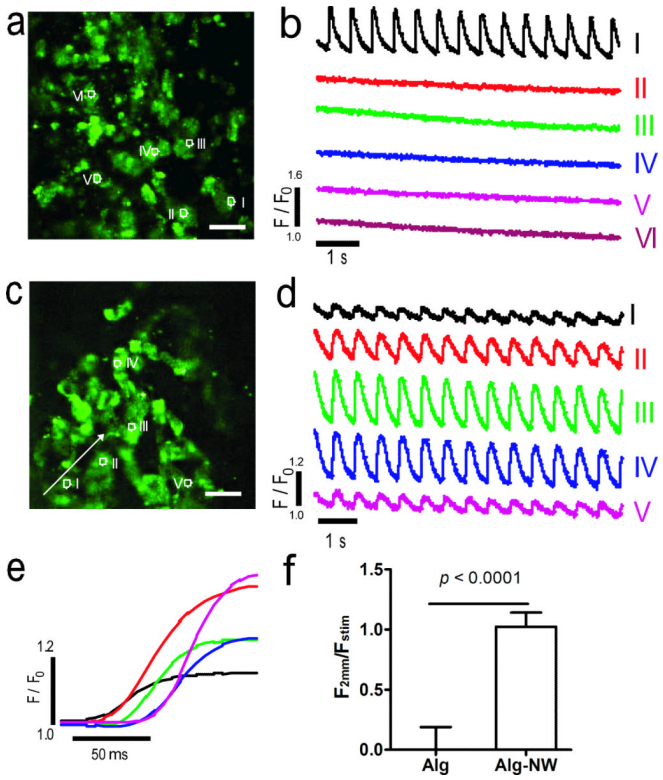

Figure 5. Calcium transient propagation within the engineered tissues

Calcium transient was assessed at specified points (white circles) by monitoring calcium dye fluorescence (green) **a,** Sites monitored in pristine scaffold where site I is the stimulation point. **b,** Calcium transients were only observed at the stimulation point in the unmodified scaffold. F/F_0 refers to measured fluorescence normalized to background fluorescence. **c,** Sites monitored in an Alg-NW scaffold. The stimulation point was 2 mm diagonally to the lower left of point I (i.e. off the figure). The white arrow represents the direction of propagation. **d,** Calcium transients were observed at all points. **e,** Comparison of the initial time courses of single signals from sites I–V in panel d. f. Quantification of calcium transients (by relative fluorescence) from all samples (n=6 in each group). Bars represent signal maximum transient 2 mm from the stimulation site (F_{2mm}), normalized to the signal maximum at the simulation site (F_{stim}). Scale bar in a, c = 100 μm.